Rapid acidification of mode and intermediate waters in the southwest Atlantic Ocean.

Lesley A. Salt[1*], Steven M. A. C. van Heuven[2**], Maaike E. Claus[3], Elizabeth M. Jones[4], and Hein J. W. de Baar[1,3]

[1]{Royal Netherlands Institute for Sea Research, Landsdiep 4, 1797 SZ, Texel, The Netherlands}
[2]{Centre for Isotope Research, University of Groningen, Nijenborgh 4, 9747 AG, Groningen,
The Netherlands}
[3]{Department of Ocean Ecosystems, University of Groningen, Nijenborgh 7, 9747 AG, Groningen, The Netherlands}
[4]{Alfred Wegener Institute for Polar and Marine Research, 120161, D-27515, Bremerhaven, Germany}

*now at {CNRS, UMR 7144, Equipe Chimie Marine, Station Biologique de Roscoff, Place Georges Teissier, 29680 Roscoff, France}

**now at {Alfred Wegner Institute, Climate Sciences Department, Postfach 120161, 27515 Bremerhaven, Germany}

Correspondence to: L. A. Salt (lesley.salt@sb-roscoff.fr)

Abstract

Observations along the southwest Atlantic WOCE A17 line made during the Dutch GEOTRACES-NL program (2010-11) were compared with historical data from 1994 to quantify the changes in the anthropogenic component of the total pool of dissolved inorganic carbon (ΔC_{ant}). Application of the extended Multi Linear Regression (eMLR) method shows that the ΔC_{ant} from 1994 to 2011 has largely remained confined to the upper 1000 dbar. The greatest changes occur in the upper 200 dbar in the SubAntarctic Zone (SAZ), where a maximum increase of 37 μmol kg^{-1} is found. South Atlantic Central Water (SACW) experienced the highest rate of increase in C_{ant}, at 0.99±0.14 μmol kg^{-1} y^{-1}, resulting in a maximum rate of decrease in pH of 0.0016 yr^{-1}. The highest rates of acidification relative to ΔC_{ant}, however, were found in SubAntarctic Mode Water (SAMW) and Antarctic Intermediate Water (AAIW). The low buffering capacity of SAMW and AAIW combined with their relatively high rates of C_{ant} increase of 0.53±0.11 μmol kg^{-1} y^{-1} and 0.36±0.06 μmol kg^{-1} y^{-1}, respectively, has lead to rapid acidification in the SAZ, and will continue to do so whilst simultaneously reducing the chemical buffering capacity of this significant CO_2 sink.

1 Introduction

The Atlantic Ocean contains the largest store of anthropogenic carbon (C_{ant}) of all the world's oceans, accounting for approximately 38% of the total C_{ant} inventory (Sabine et al., 2004). Within the Atlantic, the North Atlantic has been found to be responsible for the majority of the uptake of C_{ant}, due to the formation of North Atlantic Deep Water (NADW)(Lee et al., 2003; Sabine et al., 2004). However, a recent Atlantic basin inventory analysis indicates that in the past decade the South Atlantic has been more effective at sequestering C_{ant} (Wanninkhof et al., 2010) than the North Atlantic. These authors calculated a rate of increase of the North Atlantic inventory of 1.9 Pg C decade^{-1}, whereas the South Atlantic inventory grew at a rate of 3.0 Pg C decade^{-1}. Calculations by Ríos et al. (2012) indicate that the southwestern Atlantic Ocean dominates the South Atlantic sink of C_{ant}, with a storage rate of 0.25±0.035 Pg C decade^{-1}. Quantifying the exact rate of increase in anthropogenic carbon in ocean waters is inherently problematic due to the highly variable nature of DIC within the ocean and the relatively small fraction of total dissolved inorganic carbon (DIC) that the anthropogenic component represents (~3%; Ríos et al., 2010). In the past decade a number of methods for calculating the increase in C_{ant} ($\Delta C_{ant)}$ between reoccupation of ocean transects have been developed (TrOCA, φC_T^0, eMLR). Despite the differing approaches and assumptions, there is overall coherence in the determinations of the anthropogenic component of inorganic carbon in the Atlantic Ocean (Lee et al., 2003; Vázquez-Rodríguez et al., 2009a; Peng et al., 2010; Wanninkhof et al., 2010).

The southwest Atlantic has been occupied several times over the past 20 years and several techniques to determine C_{ant} have been applied to the WOCE '94 A17 transect by Ríos et al. (2010). These methods included ΔC* (Gruber et al., 1996), Tracer combining Oxygen, inorganic Carbon and total Alkalinity (TrOCA)(Touratier et al., 2007), φCT° (Vázquez-Rodríguez et al., 2009a), and Transit Time Distributions (TTD)(Waugh et al., 2006) and showed general conformity in the distribution of C_{ant}. The presence of the western boundary current in the South Atlantic Ocean means that the C_{ant} signal penetrates deeper and is larger in the western half of the basin compared to the eastern half (Wanninkhof et al., 2010; Ríos et al., 2010; Vázquez-Rodríguez et al., 2009a). Similarly, Murata et al. (2008) show that the C_{ant} signal in SubAntarctic Mode Water (SAMW) can be ~7 μmol kg^{-1} higher west of 15°W compared to the east. Mode and intermediate water formation constitute a major pathway of C_{ant} into the South Atlantic Ocean interior (McNeil et al., 2001; Sabine et al., 2004). The SAMW is formed in the Subantarctic Zone (SAZ), between the Subtropical Front (STF) and subAntarctic Front (SAF), where a calculated anthropogenic CO_2 uptake of 0.07 – 0.08 PgC yr^{-1} occurs (Sabine et al., 1999; McNeil et al., 2001). A total CO_2 sink of 1.1 Pg C yr^{-1} has been calculated by McNeil et al. (2007) for the SAZ, making it the largest CO_2 sink in the Southern Ocean and a significant sink for anthropogenic atmospheric CO_2.

The increase in DIC that results from the uptake of anthropogenic CO_2 from the atmosphere leads to increasing proton, bicarbonate ion and carbon dioxide concentrations ($[H^+]$, $[HCO_3^-]$,$[CO_2]$) and decreasing carbonate concentrations ($[CO_3^{2-}]$), a process referred to as *ocean acidification*. Sabine et al. (2004) state that approximately 50% of the total amount of C_{ant} in the world's oceans resides in the upper 400 m. The associated decrease in pH has been calculated as 0.1 pH units in the surface ocean relative to pre-industrial times (Orr et al., 2005) and is ongoing. Observations have found acidification rates of 0.0016±0.0001 yr^{-1} and 0.0012±0.002 yr^{-1}, in the North Atlantic Ocean, for Subarctic Intermediate Water (SAIW) and SubPolar Mode Water (SPMW), respectively (Vázquez-Rodríguez et al., 2012). Data from the European Time Series in the Canary Islands (ESTOC) station shows significantly higher rates of pH decrease in surface waters of 0.0017 ± 0.0004 yr^{-1}, for the time period

1995 to 2004 with notable influence from regional climatic forcing (Santana-Casiano et al., 2007). Acidification rates that deviate from the rate that is expected from C_{ant} increases alone have been observed in upper Labrador Sea Water (uLSW), SAIW, and eastern North Atlantic Central Water (eNACW) (Vázquez-Rodríguez et al., 2012). These variations have been attributed to a combination of climatic and biological effects. The greater sensitivity of some water masses to acidification has been well documented by González-Dávila et al. (2011) through the application of the buffering factors described by Egleston et al. (2010). González-Dávila et al. (2011) highlighted waters originating at high latitudes as particularly sensitive to increases in the concentration of dissolved CO_2 ([CO_2 (aq)]), in particular Antarctic Intermediate Water (AAIW) and upper Circumpolar Deep Water (*u*CDW) due to low total alkalinity (A_T) to DIC ratios.

A number of the biological consequences of ocean acidification are related to the changes in carbonate, and thus calcium carbonate ($CaCO_3$), ion concentration. Carbonate ions are used by marine calcifying organisms to form both varieties of calcium carbonate: aragonite (e.g. by pteropods) and calcite (e.g. by coccolithophores and foraminifera). Aragonite is the less metastable form of $CaCO_3$ resulting in a saturation horizon (Ω_{Ar}=1) approximately 2 km shallower than that of calcite in the South Atlantic Ocean, below which depth the $CaCO_3$ present will be in dissolved form. A number of experiments have observed shell dissolution in pteropods incubated at elevated partial pressure of CO_2 (pCO_2) (Orr et al., 2005; Lischka et al., 2011) associated with a lowering of the aragonite saturation state. Recently similar results have been observed *in situ* in the Southern Ocean (Bednaršek et al., 2012), indicating that species are already being affected by C_{ant} accumulation. Organisms that use aragonite are thus much more vulnerable to decreases in [CO_3^{2-}] driven from the surface increase in [CO_2].

This study examines the increase of C_{ant} in the southwest Atlantic Ocean between two occupations of the WOCE A17 line, which took place in 1994 and 2010/11. We calculate the changes in C_{ant} (ΔC_{ant}) in the different water masses and subsequently examine the pH changes driven by the invasion of anthropogenic carbon between WOCE ‘94 A17 and GEOTRACES-NL (2010/2011). These results are furthermore put into context with regard to the differing buffering capacities of individual water masses.

2 Data

The two datasets used in this study are the results from the CO_2 survey data from the WOCE '94 A17 section (public data at: http://cdiac.ornl.gov/oceans/woce_a17c.html) and the Dutch West Atlantic GEOTRACES program, completed in 2011 (GEOTRACES-NL (2010/2011)(public data available at: http://www.bodc.ac.uk/geotraces/data/idp2014/). The respective stations from the two campaigns are shown in Fig. 1. The GEOTRACES-NL (2010/2011) section was carried out in two parts. The shown stations north of the equator were occupied in July 2010 by the Dutch RV Pelagia (expedition 64PE321, from Hamilton, Bermuda to Fortaleza, Brazil), and the southern hemisphere was sampled during March 2011 by the British RRS James Cook (JC057, from Punta Arenas, Chile to Las Palmas, Gran Canaria).

2.1 WOCE '94 A17 measurements

The WOCE '94 A17 section was similarly carried out in austral autumn and this data has undergone rigorous quality control (Key et al., 2010). The data report is available from 'http://cdiac.ornl.gov/oceans/ndp_084/' (Ríos et al., 2005), where an offset of -8 μmol kg^{-1} in the total alkalinity (A_T) data has been reported and corrected for in this study. From this dataset only the stations where data for both A_T and DIC are available, were used. This resulted in a total of 59 stations and 1683 datapoints. For a detailed analysis of the WOCE occupation we refer the reader to Ríos et al., (2010).

2.2 GEOTRACES-NL (2010/11) measurements

2.2.1 Dissolved inorganic carbon and total alkalinity

During the GEOTRACES-NL (2010/2011) cruises, for measurements of DIC and A_T, water samples of 600 ml were collected from throughout the water column, from 24 Niskin samplers mounted onto a CTD rosette, following standard operating procedures (Dickson et al., 2007). At least two duplicates samples were collected at each station, from different parts of the profile. Samples were analyzed immediately after collection on a VINDTA 3C (Versatile INstrument for the Determination of Total Alkalinity, Marianda, Kiel) instruments, simultaneously. This system determines DIC by coulometric titration using a coulometer

(Johnson et al., 1987) and determines A_T by potentiometric titration with 0.1M hydrochloric acid (Mintrop et al., 2000). Quality control was performed through regular measurements of certified reference material (CRM, Batch #100) supplied by Dr. Andrew Dickson at Scripps Institute of Oceanography (San Diego, California). Based on the measurements performed on the CRM throughout both cruises, DIC was measured with a precision of ±1.0 μmol kg^{-1} and the precision of A_T was ±1.1 μmol kg^{-1}.

2.2.2 Ancillary parameters

Dissolved oxygen samples were collected from a minimum of three depths throughout the water column for CTD sensor calibration. Inorganic nutrients (PO_4, $Si(OH)_4$, NO_3) were analyzed following the methods of Grasshoff et al. (1983). In every run a control and a natural sterilized, Reference Nutrient Sample (RMNS Kanso, Japan) were measured for validation. Precision was estimated to be ± 0.01, 0.2, and 0.2 μmol l^{-1} for PO_4, $Si(OH)_4$, and NO_3, respectively. Values of salinity are reported on the practical salinity scale.

2.2.3 pH Calculations

From DIC, A_T and supplementary data (salinity, temperature, pressure, $Si(OH)_4$, PO_4), the pH and pCO_2 were also calculated in-situ for both datasets using CO2_SYS (Lewis and Wallace, 1998) adapted for Matlab (van Heuven, 2011a), applying the acid dissociation constants of Mehrbach et al. (1973, refit by Dickson and Millero, 1987), and the KSO_4 constant of Dickson (1990). Identical calculation were carried out on A_T and DIC data from both the WOCE ’94 A17 and GEOTRACES-NL (2010/2011) datasets, with the resulting pH reported on the total pH scale.

2.3 Deepwater consistency between WOCE and GEOTRACES

In a later section, we employ the extended Multi Linear Regression (eMLR) method (Wallace, 1995; Friis et al., 2005) to infer ΔC_{ant} between the two cruises. The eMLR method considers various biogeochemical properties (in this case, salinity, DIC, NO_3, $Si(OH)_4$ and apparent oxygen utilization ($AOU=[O_2]_{sat}-[O_2]_{obs}$)) and is particularly sensitive to large scale (‘secular’) changes in the distributions of these properties, as well as to analytical biases in their measurement. In order to assess the magnitude and distributions of these changes, we gridded the values of salinity, DIC, NO_3, $Si(OH)_4$ and AOU of each dataset and the gridded

WOCE dataset was subtracted from the GEOTRACES grid. Grid spacing was every 2 degrees of latitude, with 80 layers in the vertical direction, with increased density towards the surface. In the *lower* Circumpolar Deep Water (*l*CDW; conceivably the most stable water mass in the section) the differences average -0.01±0.015 (salinity), -4.2±12.1 µmol kg^{-1} (DIC), -1.92±0.78 µmol kg^{-1} (NO_3), -5.05±3.3 µmol kg^{-1} ($Si(OH)_4$) and -3.13±3.9 µmol kg^{-1} (AOU).

3 Methods

3.1 eMLR and C_{ant} Calculations

There are two general carbon data-based approaches for studying the increasing oceanic C_{ant}. The first approach uses back-calculation techniques to obtain an estimate of pre-industrial DIC concentration against which to compare current measurements. Methods from the second approach aim to determine the part of change in DIC between two specific time periods that is attributable to anthropogenic invasion. One example of each approach is employed in this study; eMLR (Friis et al., 2005) and φC_T (Vázquez-Rodríguez et al., 2009a, 2009b). Various comparison and evaluations of these and other methods are available in the literature (Levine et al., 2008; Yool et al., 2010; van Heuven et al., 2011b; Sabine and Tanhua, 2010).

3.1.1 ΔC_{ant} from eMLR

The multi-linear regression approach to estimating anthropogenic CO_2 invasion was introduced by Wallace (1995). It involves using a number of biogeochemical properties, known to be related to DIC, to obtain a model of the observed DIC. As the relationships between DIC and these properties are expected not to change over time, the same statistical relationships can be applied to a second dataset of later date. Differences between the thus 'predicted' DIC and the observed DIC are attributed to the invasion of anthropogenic CO_2. In the extended version (eMLR) developed by Friis et al. (2005), which is applied here, the DIC from two datasets is fitted to the same selection of properties from both datasets, and the difference between parameter coefficients is assumed to be predictive of the difference in C_{ant} between the two cruises:

$$\Delta C_{ant}^{\ eMLR} = DIC^{\ MLR2,t2} - DIC^{\ MLR1,t1} \qquad (1)$$

$$= (a_2 - a_1) + (b_2 - b_1)\ SiO_{2t2} + (c_2 - c_1)\ NO_{3t2} + (d_2 - d_1)\ AOU_{t2} + (e_2 - e_1)$$

$$S_{t2} + (f_2 - f_1)\, T_{t2} + (g_2 - g_1)\, P_{t2} \qquad (2)$$

Following equation 2, we apply the backward calculation technique as the DIC data from the more recent GEOTRACES-NL (2010/2011) cruise demonstrates a greater precision. The properties used to predict DIC in the WOCE '94 dataset results in an R^2 value of 0.97 and a root mean square error (rmse) of 10.7 µmol kg^{-1}. For the GEOTRACES-NL (2010/2011) dataset a R^2 of 0.98 was obtained and a rmse of 9.9 µmol kg^{-1} (Fig. 2).

The eMLR regressions were applied along isopycnals intervals, as the preferred method of water movement from the surface into the ocean interior is along surfaces of constant density. It thus follows that waters occupying the same density band share a common formation history and can be described by a single equation. Isopycnal bands were chosen based on temperature-salinity plots of the water masses and the amount of data occupying each interval. The coefficients and accompanying statistics from each isopycnal interval are displayed in Table 1(a) and (b) for the 1994 and 2010/11 regressions, respectively. The residuals of each fit are shown in Fig. 2, with the 2011 dataset showing an average of 2.1 µmol kg^{-1} in the more stable deeper waters (>2000 dbar). In comparison, the WOCE '94 A17 dataset shows a deep water (>2000 dbar) column average residual of 3.17 µmol kg^{-1}, which we attribute to less precise measurements in the earlier dataset. Pressure was included in the regression to avoid skewing (over depth) of the residuals of the MLR by the relatively large amount of samples located towards the surface, as mentioned by Hauk et al. (2010).

3.1.2 C_{ant} from $\varphi C_T°$

The $\varphi C_T°$ method is a back-calculation approach that uses stoichiometric ratios from biogeochemical processes to account for the addition of DIC in the water column resulting from organic matter remineralization and calcium carbonate dissolution, since the time of water formation (Vázquez-Rodríguez, 2008; Vázquez-Rodríguez et al. 2009a). It is based on the general principle of 'preformed DIC' (or C_T^o) of Brewer (1978) and ΔC^* of Gruber et al. (1996). The main advantage of this method is that it considers the non-steady state of A_T and pCO_2 in the subsurface reference layer.

3.2 Buffer Factors

The *revelle factor* was originally described by Revelle and Suess (1957) and quantified the attenuated response of increasing DIC impacted by increasing pCO_2, or vice versa. This work has been built upon by Egleston et al. (2010), who outlined six expressions that define how [CO_2], [H^+], and Ω_{Ar} or Ω_{Ca}, are impacted by changes in DIC or A_T. The following three expressions for the buffer factors relating to DIC were applied to the GEOTRACES-NL (2010/2011) and WOCE ’94 A17 southwest Atlantic sections (Equations (3-4) and (6-7) are taken from Egleston et al., (2010), however, Equation (5) and (8) are taken from Álvarez et al., (2014), who identified and corrected a typo in the definitions of Egleston et al., 2010).

$$\gamma\mathrm{DIC} = \mathrm{DIC} - \mathrm{Alk_C}^2/S, \qquad (3)$$

$$\beta\mathrm{DIC} = \mathrm{DIC} \times S - \mathrm{Alk_C}^2/\mathrm{Alk_C}, \qquad (4)$$

$$\omega\mathrm{DIC} = \mathrm{DIC} - \{\mathrm{Alk_C} \times (2 \times [CO_2] + [HCO_3^-])/P\}, \qquad (5)$$

where

$$\mathrm{DIC} = [CO_2] + [HCO_3^-] + [CO_3^{2-}], \qquad (6)$$

$$\mathrm{Alk_C} = [HCO_3^-] + 2[CO_3^{2-}], \qquad (7)$$

$$P = [HCO_3^-] - \{[H^+][B(OH)_4^-]/K\mathit{hb} + [H^+]\} - [H^+] + [OH^-], \qquad (8)$$

$$S = [HCO_3^-] + 4[CO_3^{2-}] + [H^+] + [OH^-] + \{[H^+][B(OH)_4^-]/K\mathit{hb} + [H^+]\} \qquad (9)$$

and Ω refers to the saturation state of sea water with respect to aragonite or calcite. These equations quantify the resistance to change of [CO^2] (γDIC), [H^+](βDIC) and Ω(ωDIC) in a water mass to changes in DIC. The concentrations used for the calculations were obtained from CO2SYS (Lewis and Wallace, 1998, adapted for Matlab by van Heuven, 2011a) using the same input conditions as previously mentioned (Sect. 2.2.3).

4 Hydrography of the South Atlantic Ocean

The distributions of potential temperature, salinity, AOU, silicate, A_T, and DIC of the GEOTRACES-NL (2010/2011) section are shown in Fig. 3. The large water masses have been described elsewhere (Mémery et al., 2000; Ríos et al., 2010; Wanninkhof et al., 2010), thus here the treatment is relatively concise. Located deeper than 4500 dbar throughout the section is Antarctic Bottom Water (AABW), characteristic in its high DIC and AOU. Values for DIC in this water mass range from 2243 to 2267 µmol kg^{-1}, and AOU values occupy a narrow band between 111 to 128 µmol kg^{-1}. The DIC maximum (2267 µmol kg^{-1}) and potential temperature minimum (-0.16°C) are both found in this water mass, which also shows the deep water (>1000 dbar) A_T maximum (2369 µmol kg^{-1}). These characteristics are all representative of the old age of the water mass and are caused by the large amount of organic matter remineralization which has taken place within it. The AABW can, most easily, be distinguished from the overlying *lower* Circumpolar Deep Water (*l*CDW), by the high silicate concentrations, which reach values greater than 120 umol kg^{-1} in AABW. Silicate concentrations in the deep waters (>4000 dbar) demonstrate a strong covariance with A_T (R^2=0.95), which has been previously noted and stems from the simultaneous dissolution of opaline and calcium carbonate shells from the hard tissue of organisms (Pérez et al., 2002).

The *l*CDW has a core at approximately 3500 dbar at 50ºS, above which it merges into *upper* Circumpolar Deep Water (*u*CDW), with its respective core identified by an oxygen minimum at approximately 1500 m (Mémery et al., 2000). Both branches of CDW display properties similar to that of AABW, as they represent a mixture of AABW and Weddell Sea Deep Water (Wong et al., 1999; Orsi et al., 1999). The *u*CDW and *l*CDW share isopycnals with *upper* North Atlantic Deep Water (*u*NADW) and *lower* North Atlantic Deep Water (*l*NADW), respectively, in the northern half of the section (Fig. 3a). The *u*CDW and *u*NADW, occupy the density band between σ_θ>27.4 and σ_3<41.47, with the front between the two water masses found at approximately 26ºN (Mémery et al., 2000). The NADW has been more recently ventilated than CDW and is thus distinguished by lower AOU values of ~60 µmol kg^{-1} and DIC values lower than 2200 µmol kg^{-1}. The deeper *l*NADW can be separated from *u*NADW through higher silicate values, which rise to 40 µmol kg^{-1}, whereas *u*NADW has maximum silicate concentrations of 20 µmol kg^{-1} (Fig. 3d). The A_T values are also lower (~20 µmol kg^{-1}) in *u*NADW compared to *l*NADW.

The Antarctic Intermediate Water (AAIW) enters the section at 200 dbar just south of 48°S, identifiable as a tongue of water with very low salinity and A_T (34.05 and 2275 µmol kg^{-1}, respectively)(Fig. 3b). The AAIW lies above *u*CDW and below SubAntarctic Mode Water (SAMW) (Peterson and Whitworth, 1989). This water mass is carried northward at intermediate depths between σ_θ>27.1 and σ_θ<27.4 (Ríos et al., 2012) from south of the SAF. In the southwestern Atlantic Ocean AAIW extends further north than in other oceans, due to the western boundary current along the coast of South America (Talley, 1996). The AAIW is a relatively young water mass and has AOU values comparable to NADW (~50 – 100 µmol kg^{-1}), however, it can be distinguished from *u*NADW, in its northward reaches, by its elevated silicate concentrations. Situated above the AAIW, the SAMW is often considered a component of the AAIW (McCartney, 1977). This water mass can be easily identified by the tracer Si* = $[Si(OH)_4]$-$[NO_3^-]$ which has values from -10 to -15 μmol kg^{-1} in regions of SAMW formation (Sarmiento et al., 2004). The SAMW formation region is located just south of 47ºS in the Subantarctic Zone (SAZ), north of the SAF (McCartney, 1977) where deep winter mixing forms this high-oxygen water mass.

We locate the Subtropical Front (STF) at ~41°S, where there is a steep gradient in salinity in the surface 200 dbar. North of the STF, in the surface, and extending northward to a density of σ_θ<26.5 kg m^{-3}, is South Atlantic Central Water (SACW; Ríos et al., 2012), heavily depleted in silicate, and with elevated salinity and A_T. Against this background, the two Amazon plumes are very distinct at 5°N and 15°N with salinity and A_T values as low as 34.11 and 2265 μmol kg^{-1}, and 32.3 and 2157 μmol kg^{-1}, respectively. The maximum values of both salinity and A_T correspond with South Atlantic Central Water (SACW) in the subtropics (17°S), reaching absolute maxima of 37.5 and 2456 μmol kg^{-1}, respectively, at 50 dbar depth. The subtropical part of the SACW that features high salinity and A_T is often referred to as the Salinity Maximum Water (SMW). In this study we make no distinction between SMW and SACW.

5 Results and discussion

5.1 Anthropogenic carbon in the southwest Atlantic Ocean

The distribution of C_{ant} in 2011, calculated using the $\varphi C_T°$ method (Vázquez-Rodríguez, 2008; Vázquez-Rodríguez et al. 2009a), and the calculated increase in C_{ant} (ΔC_{ant}) from 1994 to 2011, obtained from an eMLR analysis, are shown in figures 4a and 4b, respectively. Both distributions show good consistency with previous studies (Ríos et al., 2010; Wanninkhof et al., 2010; Ríos et al., 2012) and are not dissimilar from each other, with areas of high C_{ant} also demonstrating the highest ΔC_{ant} from 1994-2010/11. The total C_{ant} (Fig 4a) values show an increase in the surface waters compared to that of Rios et al. (2010), calculated from the WOCE ’94 A17 dataset, which is consistent with the calculated ΔC_{ant} presented here (Fig 4b). The general pattern is that from 1994 to 2011 the most evident increase in C_{ant} occurred in the upper 1000 dbar, particularly in the southern half of the section, with the ΔC_{ant}

increasing towards the surface. The atmosphere is the main source of C_{ant} to the ocean, thus it follows that the waters most recently in contact with the atmosphere will show the greatest ΔC_{ant}. Within the surface waters (<100 dbar) of the section the ΔC_{ant} gradually decreases northwards in a linear relationship with latitude ($R^2 = -0.74$) to a concentration of 0 µmol kg^{-1} just north of the equator (~5°N). Despite containing large quantities of C_{ant} (Fig. 4a), low ΔC_{ant} values (<5 µmol kg^{-1}) have been previously noted in the tropical Atlantic region, to a depth of 200 dbar, similar to that observed here (Schneider et al., 2012). The same authors have suggested that greater precipitation in the inter-tropical convergence zone can cause errors in the surface C_{ant} determinations in the tropical Atlantic, due to the related increase in revelle factor. In the section presented here the Amazon outflow can also be seen in salinity values, thus a variation in freshwater input may also contribute to errors in the method.

The largest increase (up to 37 µmol kg^{-1}) in surface waters was found in the SAZ, just south of 45°S, in agreement with the findings of Wanninkhof et al. (2010). The steepest vertical gradient of ΔC_{ant} is found in the same region, at ~47°S just north of the SAF, where over a depth range of 0-600 dbar the ΔC_{ant} decreases from 37 to 0 µmol kg^{-1}. Further north, the deepest penetration of positive ΔC_{ant} values in the southern half of the section is found at 1200 dbar in the STZ, between 25ºS and 40ºS. The ΔC_{ant} zero-contour shoals southward of 35°S to ~600 dbar at 50ºS, coinciding with the lower limits of AAIW, as has been noted in other ocean basins (Sabine et al., 2004). In the northern half of the section, the deepest limit of ΔC_{ant} penetration in AAIW reaches a depth of ~700 dbar at 15ºS and north of the equator the AAIW signal becomes distorted as it mixes with NADW. The NADW shows near-zero concentrations of ΔC_{ant} throughout its extent, with the exception of the *u*NADW in the equatorial region, which show ΔC_{ant} values up to 5 µmol kg^{-1}. In *l*NADW and the other deep and bottom waters (AABW, *l*CDW), ΔC_{ant} shows no change or a tendency to negative values.

To estimate the rate of increase of C_{ant} in each water mass we identified their respective cores (Fig. 3b) using the water mass descriptions given in Mémery et al. (2000) and Ríos et al. (2012) and averaged their values of ΔC_{ant}. Assuming a constant yearly increase, we then divided this total increase by 17 to obtain the rate of yearly increase of C_{ant} over the period 1994 to 2011. The calculated values are shown in Table 2 with those of Ríos et al. (2012) for comparison. The highest rates of increase were found in SACW and SAMW with C_{ant} increase rates of 0.99±0.14 μmol kg^{-1} y^{-1} and 0.53±0.11 μmol kg^{-1} y^{-1}, respectively. The latter value shows good consistency with that calculated by Ríos et al. (2012; 0.53±0.02 μmol kg^{-1} y^{-1}). However, there is a notable difference of 0.09 μmol kg^{-1} y^{-1} between the increase for SACW calculated here and that of 0.90±0.04 μmol kg^{-1} y^{-1} (Ríos et al., 2012). As this is a surface water mass, and our study utilized data collected 6 years after that used for comparison in Ríos et al. (2012), we corrected the ΔC_{ant} accordingly. Assuming equilibration between the atmosphere and ocean we corrected our ΔC_{ant} value for the additional DIC increase caused solely by atmospheric increases over the last 6 years. The resulting calculated $C_{ant}^{1994\text{-}2005}$ increase rate was 0.92±0.14 μmol kg^{-1} y^{-1}, making our result consistent with the previous estimate. As such, we attribute the difference in calculated ΔC_{ant} increase rates in SACW to the increase in DIC driven by higher atmospheric pCO_2 concentrations in 2010/11.

Despite the similarities in formation history between SAMW and AAIW, the latter shows a much lower C_{ant} increase rate of 0.37±0.06 umol kg^{-1} yr^{-1}. The discrepancy between the C_{ant} increase rates in these two water masses is in line with the differences in air-sea CO_2 flux in the region (McNeil et al., 2007). In the SAZ a combination of biological production and temperature variability leads to a large seasonal signal of pCO_2. The SAMW is formed in the SAZ, where there is high biological production in spring and summer and wintertime cooling of surface waters. The wintertime cooling effect on the solubility of CO_2 is sufficient to counteract the increase in DIC from mixing, resulting in a strong year-round CO_2 sink. South of the SAF, where AAIW is formed, similar processes operate, however the biological production is lower, and convective wintertime mixing brings up high-DIC waters, thus reducing the CO_2 sink (McNeil et al., 2007). It has also been shown that in the Indian Ocean the formation rate of AAIW is less than that of SAMW, which facilitates more efficient sequestration of C_{ant} by the latter (Hartin et al., 2011).

Modest increase rates of 0.33±0.07 μmol kg^{-1} y^{-1} and 0.20±0.03 μmol kg^{-1} y^{-1} were calculated for *u*CDW and *u*NADW, respectively. Both these water masses have been fairly recently ventilated, allowing modest increases in ΔC_{ant}. The increase rate for *u*NADW is in line with values found by Perez et al. (2010). Due to the very low ΔC_{ant} values found in *l*NADW and *l*CDW, their respective increase rates are not significant and are not discussed further. In contrast to our calculated ΔC_{ant}, a number of studies have found increasing concentrations of C_{ant} in AABW (Murata et al., 2008; Vázquez-Rodríguez et al., 2009a; Brown et al., 2010). However, it has been noted previously that it is absent in eMLR analyses (Wanninkhof et al., 2010). The distributions of C_{ant} in AABW presented in Vázquez-Rodríguez et al. (2009a) also indicate that C_{ant} concentrations have not yet spread further north than 50ºS, potentially explaining its absence in our analysis.

5.2 Associated changes of pH

Assuming no changes of A_T between the WOCE '94 A17 and GEOTRACES-NL (2010/2011) occupations, we use the ΔC_{ant} calculated by eMLR and the measured A_T during GEOTRACES-NL (2010/2011) to calculate the anthropogenic driven change in pH from 1994 to 2011 ($\Delta pH^{1994\text{-}2011}$). From the application of the φC_T^0 method of anthropogenic carbon determination (Sect. 2.3.2) to the WOCE '94 A17 dataset, we obtain the total C_{ant} signal from pre-industrial times to 1994 (Fig. 4a). The C_{ant} value allows the calculation of the decline in pH, which has been caused by increasing C_{ant}, during this time period (from pre-industrial times to 1994: ΔpH^{1994}). The average surface (<250 dbar) ΔpH^{1994} across the section was -0.08, which is just under the predicted, general surface ocean decrease of 0.1 (Orr et al., 2005). The ocean interior experienced relatively small ΔpH^{1994}, however, the change was accompanied by a significant shoaling of the aragonite saturation horizon, most notably in the southern half of the section (Fig. 4c). From pre-industrial times to 1994, south of the SAF, at ~49°S, the aragonite saturation horizon rose by ~250 m whereas further north, at 25°S, it has risen just 200 m. The change was almost imperceptible north of the Equator. From 1994 to 2011, $\Delta pH^{1994\text{-}2011}$, there is a further decline of 0.03 units, making the total surface ΔpH^{2011} -0.11 units since pre-industrial times. Thus, of the total decrease since pre-industrial times to the present day, 27% occurred within the past 17 years. However, we can detect no notable change to the aragonite saturation horizon over the past 17 years (Fig. 4c). Historically, the uptake of C_{ant} by the surface ocean was relatively gradual, which allowed it to be well distributed throughout the water column. In contrast, the effects of the more recent, steeply increasing, anthropogenic acidification have not yet significantly penetrated into the deeper ocean.

The distribution of $\Delta pH^{1994\text{-}2011}$ across the section broadly follows the C_{ant} increases (compare Figs 4b 4c), as expected under the assumption of constant A_T. If we further assume a constant decrease over the 17 years, the yearly acidification rates were calculated from $\Delta pH^{1994\text{-}2011}$ and identified for each water mass core, as done for the yearly C_{ant} increases (Table 2). The highest rates of acidification were found in the surface waters, where we also observe the greatest rates of C_{ant} increase, with SACW showing a rate of pH decrease of 0.0016 yr^{-1}. The latter value is in line with that calculated for the same water mass on the eastern side of the North Atlantic Ocean at the ESTOC site (0.0017 yr^{-1}) for the period 1995 to 2004 (Santana-Casiano et al., 2007; González-Dávila et al., 2011). The SAMW demonstrates the next greatest rate of decline of 0.0014 y^{-1}, followed by AAIW and *u*CDW both showing acidification rates of 0.001 yr^{-1}, which are comparable with values from other recently ventilated water masses in the North Atlantic: acidification rates of 0.0019 yr^{-1} and 0.0012 yr^{-1} have been reported for SubArctic Intermediate Water and SubPolar Mode Water, respectively (Vázquez-Rodríguez et al., 2012). The lowest non-zero acidification rate of 0.0005 yr^{-1} is found in *u*NADW.

5.3 Buffering Capacity

The continuing uptake of atmospheric CO_2 gradually depletes the naturally available carbonate ion in the surface ocean thereby decreasing the capacity to 'buffer' further CO_2 uptake and leading to the gradual acidification of the seawater. The extent to which the pH is affected by the increase of DIC is dependent upon several properties, including temperature, pressure, and A_T, which together determine the *buffering capacity* of the water. As DIC increases, assuming no other changes take place, the buffering capacity of the water is reduced as $[CO_3^{2-}]$ decreases and $[CO_2]$ increases. The A_T is not altered by the flux of atmospheric CO_2 into the ocean. However, A_T is affected by biological processes, notably the dissolution and formation of calcium carbonate, with dissolution dominating in deep waters and formation playing a more important role in the surface. Table 2 quantifies the extent to which the calculated ΔC_{ant} have impacted pH in the water masses of the southwest Atlantic Ocean. Examination of this table clearly shows that the rate of acidification per µmol kg^{-1} of DIC is not equal between water masses. The SAMW, a relatively fresh, low alkalinity water mass, has an acidification rate of -0.0014 yr^{-1}, which is 88% of that of SACW, a warmer, more saline water mass. However, the C_{ant} increase rate of SAMW is only 54% that of

SACW. The AAIW shows the same rate of acidification as *u*CDW, however, the increase of C_{ant} in *u*CDW is 10% lower than that of AAIW. These differences can be attributed to the varying buffering capacities of the water masses.

The distributions of the revelle factor and the sensitivities of $[H^+]$(βDIC), $[CO_2]$(γDIC) and Ω_{CaCO3} (ωDIC) to changes in DIC for the southwest Atlantic are shown in Fig. 5 and given per water mass in Table 3. The highest revelle factors, which indicate the greatest sensitivities to increasing DIC (denoted by low values in figures 5b, 5c, and high values in 5d) were generally found in the deep waters. That is to say that for a given increase in DIC these waters will show large resultant changes in $[H^+]$, $[CO_2]$ and $[CO_3^{2-}]$, or aragonite and calcite saturation (Ω_{Ar}, Ω_{Ca}). Both *u*CDW and *l*CDW show very similar behavior – as expected from their similar history – however, interestingly, there is a notable difference between the buffering capacities of the two limbs of NADW. The difference is most noticeable in ωDIC, likely caused by the slightly higher A_T/DIC ratio in *l*NADW. A lower βDIC in *u*NADW denotes a greater sensitivity to acidification in response to increasing DIC concentrations. More rapid acidification in *u*NADW, compared to *l*NADW, has been observed by Vázquez-Rodríguez et al. (2012) and attributed to mixing with Labrador Sea Water (LSW), which exhibits a strong decreasing pH trend with time. The lower pH of LSW and its contribution to *u*NADW could account for the reduced buffering capacity calculated in this water mass in the southwest Atlantic Ocean.

The lowest Revelle Factor, and highest βDIC values are found in SACW, closely followed by SAMW, which despite containing large concentrations of C_{ant}, both have relatively low concentrations of DIC compared to the other water masses. The SACW and SAMW also have higher concentrations of A_T giving them greater buffering capacity. The three water masses with the greatest response in pH relative to ΔC_{ant} were AAIW, *u*CDW and *l*CDW, with βDIC values of 0.148 mmol kg^{-1}, 0.141 mmol kg^{-1}, and 0.143 mmol kg^{-1}, respectively. These water masses show the highest DIC/A_T ratios along the section as they all originate in the Southern Ocean (SO) where upwelling brings deep waters rich in $[CO_2(aq)]$ and low in $[CO_3^{2-}]$ to the surface. In addition, these waters have slightly lower salinities and thus lower borate concentrations, which further diminish their buffering capacity, also reflected in the high revelle factors (Fig. 5a). For the same DIC value the buffering capacity of AAIW is substantially lower than that of *u*CDW stemming from the low A_T of AAIW, which is also reflected in the high ωDIC values. With the current calculated rate of increase of C_{ant}, aragonite will become under-saturated in AAIW around the year 2100, when DIC concentrations reach 2208 μmol kg^{-1}. This could happen even sooner, as wintertime, storm-driven upwelling entrainment of deep waters into the surface in the SO is predicted to cause seasonal aragonite under-saturation in the region as soon as 2030, when atmospheric CO_2 levels reach ~450 ppm (McNeil and Matear, 2008).

5.4 Continued C_{ant} increase

The buffering capacity of each water mass will be reduced by increasing the DIC concentrations. To investigate how the buffering capacities of the different water masses in this section have changed over time, and will continue to do so, the DIC buffer factors of each water mass were calculated and plotted against DIC concentration (Fig. 6). Due to the large relative error of the calculated ΔC_{ant} increases in the deeper waters, these were not included. The high rate of uptake of C_{ant} by SACW means that this water mass has seen the largest decrease in buffering capacity since pre-industrial times. The βDIC value has decreased from 0.281 to 0.247 mmol kg^{-1} and Ω_{Ar} has decreased from 4.1 to 3.3. In contrast, *u*CDW has shown relatively little change due to the low values of C_{ant}. However, extrapolating our calculated C_{ant} rates of increase we predict a 33 μmol kg^{-1} increase in this water mass over the next century, which will result in a significant reduction in buffering and a pH decrease of -0.102. The buffering capacities of SAMW and AAIW follow a similar pattern to each other, however, SAMW contains a greater proportion of subtropical water than AAIW, thus it maintains a slightly higher buffering capacity than AAIW. Both AAIW and *u*CDW will see a similar increase in C_{ant} over the next century (37 and 33 μmol kg^{-1}, respectively), however, the decline in Ω_{Ar} will be 1.6 times greater in AAIW, due to higher ωDIC values. The SAMW will see approximately 54% of the increase in C_{ant} that SACW will experience, however will undergo 84% of the associated pH decline. These extrapolated predictions highlight the vulnerability of SAMW and AAIW to increasing C_{ant}, as also noted by Gonzalez-Davila et al. (2011).

The observed pattern of ΔC_{ant} in the southwest Atlantic clearly identifies the SAZ as the most effective entry point of C_{ant} into the ocean. In addition, the buffering factors of Egleston et al. (2010) explicitly show that by the end of this century the two dominant water masses in this area (SAMW and AAIW) will be the most sensitive to further C_{ant} increases. Whilst it is clear that this will accelerate the rate of acidification in these water masses, it is unclear how it will affect the CO_2 uptake in the SAZ. Assuming no changes to primary production, the increased sensitivity of SAMW to DIC changes will lead to much greater seasonal variability in the carbonate system of this water mass between the productive and non-productive period. The biological uptake of DIC in the SAZ in austral spring and summer would lead to a more dramatic decrease in surface water pCO_2, allowing a greater air-sea pCO_2 flux. Conversely, the acidification and decline in Ω_{Ar} may be detrimental to calcifying organisms in the area, as observed in the Southern Ocean (Bednarsek et al., 2012), thus limiting export via the biological pump.

The water masses SAMW and AAIW both risk further reduction in their buffering capacities by long-term variability to their physical properties. On decadal time scales a freshening of AAIW has been observed in the Pacific and Indian sectors of the Southern Ocean (Wong et al., 1999). Decadal variability has also been noted in temperature, salinity and biogeochemical parameters of SAMW (Bindoff et al., 2007; Alvarez et al., 2011), which could further diminish or enhance the buffering capacity of this water mass and thus the C_{ant} driven acidification. Variations on decadal time scales have been related to the Southern Annular Mode, the dominant climate forcing over the region (Lovenduski et al., 2007; Álvarez et al., 2011). Similarly in the North Atlantic, the North Atlantic Oscillation exerts a degree of control over the carbonate system variables and C_{ant} uptake (Santana-Casiano et al., 2007; Pérez et al., 2010). Such external controls will cause irregular C_{ant} uptake over time, as has been observed by Brown et al. (2010), making it difficult to accurately predict future C_{ant} uptake and associated changes in the buffering capacity.

6 Conclusion

The continuing uptake of C_{ant} in the southwest Atlantic has been assessed through application of eMLR to two datasets collected in 1994 and 2011. The distribution of ΔC_{ant} is comparable with previous studies of C_{ant} accumulation in the region (Ríos et al., 2010). The largest increases are found in the SAZ, just north of the SAF; a previously identified substantial CO_2 sink (Metzl et al., 1999). The SACW (0.99±0.14 μmol kg^{-1} y^{-1}), SAMW (0.53±0.11 μmol kg^{-1} y^{-1}) and AAIW (0.36±0.06 μmol kg^{-1} y^{-1}) are responsible for the greatest C_{ant} uptake, consistent with earlier studies showing them to be an effective pathway of C_{ant} into the ocean interior (Álvarez et al., 2009). The lower extent of AAIW demarks the greatest depth of penetration of C_{ant} into the ocean in the past 17 years indicating that future uptake will, similarly, be largely concentrated within the surface 1000m.

The increase in C_{ant} in the southwest Atlantic has led to acidification of water masses. The calculated C_{ant}-driven acidification is greatest in SACW, where a current rate of pH decline of 0.0016 yr^{-1} is found. However, the acidification response per μmol kg^{-1} increase in DIC is greatest in the intermediate and mode waters. We identify SAMW as the water mass with the greatest risk of rapid acidification in the future, due to a combination of its high C_{ant} uptake and its limited buffering capacity. AAIW, on the other hand, is more at risk of aragonite under-saturation due its low A_T values and resultant high ωDIC values. Continued increase of C_{ant} at the current rate calculated will lead to aragonite under-saturation in the core of AAIW around the year 2100.

Acknowledgements

We thank the captains and crews of the Research Vessel Pelagia and the Royal Research Ship James Cook. We also thank M. Álvarez and an additional anonymous referee for their helpful comments and suggestions.

References

Álvarez, M., C. Lo Monaco, T. Tanhua, A. Yool, A. Oschlies, J. L. Bullister, C. Goyet, N. Metzl, F. Touratier, E. McDonagh, and H. L. Bryden (2009), Estimating the storage of anthropogenic carbon in the subtropical Indian Ocean: a comparison of five different approaches, *Biogeosciences, 6*, 681-703.

Álvarez, M., T. Tanhua, H. Brix, C. Lo Monaco, N. Metzl, E. L. McDonagh, and H. L. Bryden (2011), Decadal biogeochemical changes in the subtropical Indian Ocean associated with Subantarctic Mode Water, *J. of Geophys. Res.*, 116, C09016, doi:10.1029/2010JC006475.

Álvarez, M., H. Sanleón-Bartolomé, T. Tanhua, L. Mintrop, A. Luchetta, C. Cantoni, K. Schroeder, and G. Civitarese (2014), The CO2 system in the Mediterranean Sea: a basin wide perspective, *Ocean Sci.*, 10, 69-92, doi:10.5194/os-10-69-2014.

Bednarsek, N., G. A. Tarling, D.C.E. Bakker, S. Fielding, E.M. Jones, H.J. Venables, P. Ward, A. Kuzirian, B. Lézé, R. A. Feely and E.J. Murphy (2012) Extensive dissolution of live pteropods in the Southern Ocean, Nature Geoscience, 5, 881-885, doi:10.1038/NGEO1635.

Bindoff, N.L., J. Willebrand, V. Artale, A, Cazenave, J. Gregory, S. Gulev, K. Hanawa, C. Le Quéré, S. Levitus, Y. Nojiri, C.K. Shum, L.D. Talley and A. Unnikrishnan, (2007), Observations: Oceanic Climate Change and Sea Level. In: Climate Change 2007: The Physical Science Basis. Contribution of Working Group I to the Fourth Assessment Report of the Intergovernmental Panel on Climate Change [Solomon, S., D. Qin, M. Manning, Z. Chen, M. Marquis, K.B. Averyt, M. Tignor and H.L. Miller (eds.)]. Cambridge University Press, Cambridge, United Kingdom and New York, NY, USA.

Brewer, P.G. (1978), Direct observation of the oceanic CO_2 increase. *Geophys. Res. Lett., 5*, 997-1000.

Brown, P. J., D. C. E. Bakker, U. Schuster, and A. J. Watson (2010), Anthropogenic carbon accumulation in the subtropical North Atlantic, *J. Geophys. Res., 115*, C04016, doi:10.1029/2008JC005043.

Dickson, A.G., and F.J. Millero (1987), A comparison of the equilibrium constants for the dissociation of carbonic acid in seawater media, *Deep Sea Res., 34*, 1733-1743.

Dickson, A.G. (1990), Standard potential of the reaction: $AgCl(s)+1/2H_2(g)=Ag(s)+HCl(aq)$, and the standard acidity constant of the ion HSO_4^- in synthetic seawater from 273.15 to 318.15 K, *J. Chem. Thermodyn., 22*, 113-127.

Dickson, A. G., Sabine, C. L., and Christian, J. R. (Eds.) (2007) Guide to best practices for ocean CO_2 measurements. *PICES Special Publications 3*, 191 pp, doi:10.1029/2006JC004051.

Egleston, E. S., C. L. Sabine, and M. Morel (2010), Revelle revisited: Buffer factors that quantify the reponse of ocean chemistry to changes in DIC and alkalinity, *Global Biogeochem. Cycles*, *24*, GB1002, doi:10.1029/2008GB003407.

Friis, K., A. Körtzinger, J. Patsch, and D. W. R. Wallace (2005), On the temporal increase of anthropogenic CO_2 in the subpolar North Atlantic, *Deep Sea Res., Part I., 52*, 681-698, doi:10.1016/j.dsr.2004.11.017.

González-Dávila, M., J. M. Santana-Casiano, R. A. Fine, J. Happell, B. Delille, and S. Speich (2011), Carbonate system in the water masses of the Southeast Atlantic sector of the Southern Ocean during February and March 2008, *Biogeosciences*, *8*, 1401-1413, doi:10.5194/bg-8-1401-2011.

Grasshof, K., M. Ehrhardt, and K. Kremling (1983), Methods of seawater analysis. Verlag Chemie GmbH, Weinheim.

Gruber, N., J.L. Sarmiento, and T.F. Stocker (1996), An improved method for detecting anthropogenic CO_2 in the oceans, *Global Biogeochemical Cycles, 10*, 809-837.

Hartin, C. A., R. A. Fine, B. M. Sloyan, L. D. Talley, T. K. Chereskin, and J. Happell (2011), Formation rates of Subantarctic mode water and Antarctic intermediate water within the South Pacific, *Deep-Sea Res. I, 158*, 524-534.

Hauck, J., M. Hoppema, R. G. J. Bellerby, C. Völker, and D. Wolf-Gladrow (2010), Data-based estimation of anthropogenic carbon and acidification in the Weddell Sea on a decadal timescale, *J. Geophys. Res., 115*, C03004, 14, doi:10.1029/2009JC005479.

van Heuven, S., D. Pierrot, E. Lewis, and D. W. R. Wallace (2011a), MATLAB Program Developed for CO2 System Calculations. ORNL/CDIAC-105b. Carbon Dioxide Information Analysis Center, Oak Ridge National Laboratory, U.S. Department of Energy, Oak Ridge, Tennessee. Doi:10.3334/CDIAC/otg.CO2SYS_MATLAB_v1.1.

van Heuven, S. M. A. C., M. Hoppema, O. Huhn, H. A. Slagter, and H. J. W. de Baar (2011b), Direct observation of increasing CO_2 in the Weddell Gyre along the Prime Meridian during 1973-2008, *Deep-Sea Research II, 58*, 2613-2635, doi:10.1016/j.dsr2.2011.08.007.

Johnson, K. M., J. M. Sieburth, P. J. Williams, and L. Brändström (1987), Coulometric total carbon dioxide analysis for marine studies: Automation and calibration, *Mar. Chem., 21*, 117-133.

Karstensen, J., and D. Quadfasel (2002), Water subducted into the Indian Ocean subtropical gyre, *Deep Sea-Res. Part II: Topical Studies in Oceanography, 49* (7-8), 1441-1457.

Key, R.M., T. Tanhua, A. Olsen, M. Hoppema, S. Jutterström, C. Schirnick, S. van Heuven, A. Kozyr, X. Lin, A. Velo, D.W.R Wallace and L. Mintrop (2010). The CARINA data synthesis project: Introduction and overview. *Earth System Science Data 2*, 105–121.

Lee, K., S. -D. Choi, G. -H. Park, R. Wanninkhof, T. -H. Peng, R. M. Key, C. L. Sabine, R. A. Feely, J. L. Bullister, F. J. Millero and A. Kozyr (2003), An updated anthropogenic CO_2 inventory in the Atlantic Ocean, *Global Biogeochemical Cycles*, *17(4)*: 1116, doi:10.1029/2003GB002067.

Levine, N. M., S. C. Doney, R. Wanninkhof, K. Lindsay and I. Y. Fung (2008) Impact of ocean carbon system variability on the detection of temporal increases in anthropogenic CO_2, *Journal of Geophysical Research*, *113*, C03019, doi:10.1029/2007JC004153.

Lewis, E. L., and D. W. R. Wallace (1998), Program developed for CO_2 system calculations, ORNL/CDIAC-105. Carbon dioxide information analysis center, Oak Ridge National Laboratory, U.S. Department of Energy, Oak Ridge.

Lischka, S., J. Büdenbender, T. Boxhammer, and U. Riebesell (2011), Impact of ocean acidification and elevated temperatures on early juveniles of the polar shelled pteropod Limacina helicina: mortality, shell degradation, and shell growth, *Biogeosciences, 8*, 919-932, doi:10.5194/bg-8-919-2011.

Lovenduski, N.S., N. Gruber, S.C. Doney and I.D. Lima (2007), Enhanced CO_2 outgassing in the Southern Ocean from a positive phase of the Southern Annular Mode, *Global Biogeochem. Cycles*, 21, GB2026, doi:10.1029/2006GB002900.

McCartney, M.S. (1977) Subantarctic Mode Water, in *A Voyage of Discovery*, edited by M. Angel. Pergamon, Elmsford, New York, pp.103-119.

McNeil, B. I., B. Tilbrook, and R. Matear (2001), Accumulation and uptake of anthropogenic CO2 in the Southern Ocean, south of Australia between 1968 and 1996, *J. of Geophys. Res., 106*, C12, 31,431-31,445.

McNeil, B. I., N. Metzl, R. M. Key, R. J. Matear, and A. Corbiere (2007), An empirical estimate of the Southern Ocean air-sea CO_2 flux, *Global. Biogeochem. Cycles, 21*, GB3011, doi:10.1029/2007GB002991.

McNeil, B. I., and R. J. Matear (2008), Southern Ocean acidification: A tipping point at 450-ppm atmospheric CO_2, PNAS, 105 (48), 18860-18864.

Mémery, L., M. Arhan, X.A. Alvarez-Salgado, M.-J. Messias, H. Mercier, C.G. Castro, and A.F. Ríos (2000), The water masses along the western boundary of the south and equatorial Atlantic, *Progress in Oceanography*, *47*, 69-98.

Metzl., N., B. Tilbrook, and A. Poisson (1999), The annual fCO_2 cycle and the air-sea CO_2 flux in the sub-Antarctic Ocean. *Tellus, 51B*, 849-861.

Mintrop, L., F.F. Perez, M. Gonzalez-Davila, M.J. Santana-Casiano, and A. Kortzinger

(2000), Alkalinity determination by potentiometry: intercalibration using three different methods, *Cienc. Marinas, 26*, 23-37.

Murata, A., Y. Kumamoto, K.'I. Sasaki, S. Watanabe, and M. Fukasawa (2008), Decadal increases of anthropogenic CO_2 in the subtropical South Atlantic Ocean along 30°S, *J. of Geophys. Res.*, 113, C06007, doi:10.1029/2007JC004424.

Orr, J.C., V.J. Fabry, O. Aumont, L. Bopp, S.C. Doney, R.A. Feely, A. Gnanadesikan, N. Gruber, A. Ishida, F. Joos, R.M. Key, K. Lindsay, E. Maier-Reimer, R. Matear, P. Monfray, A. Mouchet, R.G. Najjar, G.-K. Plattner, K.B. Rodgers, C.L. Sabine, J.L. Sarmiento, R. Schlitzer, R.D. Slater, I.J. Totterdell, M.-F. Weirig, Y. Yamanaka and A. Yool (2005), Anthropogenic ocean acidification over the twenty-first century and its impact on calcifying organisms. *Nature, 437*, 681-686.

Orsi, A. H., G. C. Johnson and J. L. Bullister (1999), Circulation, mixing, and production of Antarctic Bottom Water, *Progress in Oceanography*, *43*, 55-109.

Pai, S. –C., Gong, G., Liu, K. –K. (1993), Determination of dissolved oxygen in seawater by direct spectrophotometry of total iodine, *Mar. Chem., 41*, 343-351.

Peng, T. -H., and R. Wanninkhof (2010), Increase in anthropogenic CO_2 in the Atlantic Ocean in the last two decades, *Deep-Sea Research I*, 57, 755-770, doi:10.1016/j.dsr.2010.03.008.

Pérez, F. F., Álvarez, M., and Ríos, A. F. (2002) Improvements on the back-calculation technique for estimating anthropogenic CO_2, *Deep-Sea Research I*, *49,* 859-875.

Pérez, F. F., M. Vázquez-Rodríguez, H. Mercier, A. Velo, P. Lherminier, and A. F. Ríos (2010), Trends of anthropogenic CO_2 storage in North Atlantic water masses, *Biogeosciences*, 7, 1789-1807, doi:10.5194/bg-7-1789-2010.

Peterson, R. G., and T. Whitworth (1989), The Subantarctic and Polar Fronts in relation to deep water masses through the Southwestern Atlantic, *J. Geophys. Res., 94* (C8), 10817 - 10838.

Revelle, R. and H. Suess (1957), Carbon dioxide exchange between atmosphere and ocean and the question of an increase of atmospheric CO_2 during the past decades, *Tellus, 9*, 18-27.

Ríos, A.F., K. M. Johnson, X.A. Alvarez-Salgado, L. Arlen, A. Billant, L.S. Bingler, P. Branellec, C.G. Castro, D.W. Chipman, G. Roson and D.W.R. Wallace (2005), Carbon Dioxide, Hydrographic, and Chemical Data Obtained During the R/V Maurice Ewing Cruise in the South Atlantic Ocean (WOCE Section A17, 4 Janurary-21 March 1994), Carbon Dioxide Information Analysis Center, Oak Ridge National Laboratory, ORNL/CDIAC-148, NDP-084, pp. 1-27.

Ríos, A.F., Vázquez-Rodríguez, M., Padin, X.A., and Pérez, F.F. (2010) Anthropogenic carbon dioxide in the South Atlantic western basin. *Journal of Marine Systems*, *83,* 38-44.

Ríos, A.F., A. Velo, P.C. Pardo, M. Hoppema and F.F. Pérez (2012), An update of anthropogenic CO_2 storage rates in the western South Atlantic basin and the role of Antarctic Bottom Water, Journal of Marine Systems, 94, 197-203, doi:10.1016/j.jmarsys.2011.11.023.

Sabine, C.L., R.M. Key, K.M. Johnson, F.J. Millero, A. Poisson, J.L. Sarmiento, D.W.R. Wallace, and C.D. Winn (1999), Anthropogenic CO_2 inventory of the Indian Ocean, *Global Biogeochem. Cycles, 13*, 179-198.

Sabine, C., et al. (2004) The Oceanic Sink for Anthropogenic CO_2, *Science. 305*, 367-371.

Sabine, C.L. and T. Tanhua (2010). Estimation of Anthropogenic CO_2 Inventories in the Ocean. Annual Review of Marine Science 2(1), 175–198.

Santana-Casiano, J. M., M. González-Dávila, M.-J. Rueda, O. Llinás, and E.-F. González-Dávila (2007), The interannual variability of oceanic CO_2 parameters in the northeast Atlantic subtropical gyre at the ESTOC site, Global Biogeochemical Cycles, 21, GB1015, doi:10.1029/2006GB002788.

Sarmiento, J. L., N. Gruber, M. A. Brzezinski and J. P. Dunne (2004), High-latitude controls of thermocline nutrients and low latitude, *Nature, 427*, 56-60.

Schneider, A., T. Tanhua, A. Kortzinger, and D. W. R. Wallace (2012), An evaluation of tracer fields and anthropogenic carbon in the equatorial and the tropical North Atlantic, *Deep-Sea Res. I*, 67, 85-97.

Talley, L. D. (1996), Antarctic intermediate water in the South Atlantic. In: Wefer, G., Berger, H.H., Siedler, G., Webb, D. (Eds.), The South Atlantic: Present and Past Circulation. Springer-Verlag.

Touratier, F., L. Azouzi, and C. Goyet (2007) CFC-11, $\Delta^{14}C$ and ^3H tracers as a means to assess anthropogenic CO_2 concentrations in the ocean, *Tellus*, *59B,* 318-325.

Vázquez-Rodríguez, M. (2008). Reconstructing preformed properties and air-sea CO_2 disequilibria for water masses in the Atlantic from subsurface data: An application in anthropogenic carbon determination. PhD Thesis of University of Vigo, Spain.

Vázquez-Rodríguez, M., Touratier, F., Lo Monaco, C., Waugh, D.W., Padin, X.A., et al., (2009a) Anthropogenic carbon distributions in the Atlantic Ocean: data-based estimates from the Arctic to the Antarctic. *Biogeosciences*, *6,* 439-451.

Vázquez-Rodríguez, M., X. A. Padin, A. F. Ríos , R. G. J. Bellerby, and F. F. Perez (2009b), An upgraded carbon-based method to estimate the anthropogenic fraction of dissolved CO_2 in the Atlantic Ocean, *Biogeosciences Discusion, 6*, 4527-4571, doi:10.5194/bgd-6-4527-2009.

Vázquez-Rodríguez, M., F. F. Pérez, A. Velo, A. F. Ríos, and H. Mercier (2012), Observed acidification trends in North Atlantic water masses, *Biogeosciences, 9,* 5217-5230, doi:10.5194/bg-9-5217-2012.

Wallace, D.W.R. (1995), Monitoring global ocean carbon inventories. OOSDP Background Report No. 5, Texas A&M University, College Station, Texas, USA.

Wanninkhof, R., S. C. Doney, J. L. Bullister, N. M. Levine, M. Warner, and N. Gruber (2010), Detecting anthropogenic CO_2 changes in the interior Atlantic Ocean between 1989 and 2005, *J. Geophys. Res*., *115*, C11028, doi:10.1029/2010JC006251.

Waugh, D.W., T.M. Hall, B.I. McNeil, R. Key, and R.J. Matear (2006), Anthropogenic CO_2 in the oceans estimated using transit time distributions, *Tellus 58B*, 376-389, doi:10.1111/j.1600-0889.2006.00222.x.

Wong, A. P. S., N. L. Bindoff, and J. A. Church (1999), Large-scale freshening of intermediate waters in the Pacific and Indian oceans, *Nature*, 400, 440-443.

Yool, A., A. Oschlies, A. J. G. Nurser, N. and Gruber (2010) A model-based assessment of the TrOCA approach for estimating anthropogenic carbon in the ocean. *Biogeosciences*, *7,* 723-751.

Tables

Table 1a.

Min density	Max density	Mean Layer Depth (m)	a	Si(OH)$_4$	NO$_3$	Sal	Theta	AOU	Pressure	rmse	R^2	n
						Sigma-θ						
20.0	23.5	31	131	1.61	33.91	56.25	-4.78	-0.08	0.208	7.6	0.98	90
23.5	24.5	50	656	-1.73	14.13	42.36	-5.56	0.35	-0.011	6.3	0.95	73
24.5	25.0	53	152	-23.36	17.86	60.70	-11.33	0.22	-0.262	5.0	0.99	23
25.0	25.4	57	711	-7.00	2.69	41.06	-5.12	0.83	-0.094	5.5	0.99	45
25.4	26.2	107	157	-4.99	1.85	14.10	-	0.74	0.008	3.8	0.9	84

			7				**0.08**				**9**	
26.2	**26.4**	**160**	**1206**	**-0.35**	**1.36**	**26.14**	**-3.38**	**0.57**	**-0.017**	**2.1**	**1.00**	**45**
26.4	**26.6**	**196**	**825**	**-0.35**	**3.68**	**36.18**	**-2.15**	**0.23**	**0.003**	**2.4**	**1.00**	**72**
26.6	**26.8**	**259**	**1249**	**-0.42**	**2.77**	**24.17**	**-1.56**	**0.33**	**-0.004**	**1.7**	**1.00**	**67**
26.8	**27.0**	**310**	**1116**	**-0.33**	**2.22**	**28.72**	**-3.30**	**0.37**	**-0.012**	**1.6**	**1.00**	**109**
27.0	**27.2**	**431**	**1366**	**0.97**	**4.33**	**18.81**	**3.61**	**0.06**	**-0.002**	**1.1**	**1.00**	**112**
27.2	**27.4**	**672**	**601**	**0.45**	**3.58**	**42.68**	**-3.07**	**0.16**	**-0.004**	**2.1**	**0.99**	**96**
27.4	**27.5**	**991**	**2575**	**0.77**	**-0.38**	**-13.66**	**-3.01**	**0.72**	**0.006**	**1.4**	**0.98**	**42**
						Sigma-2						
27.5	**36.7**	**1108**	**2056**	**0.65**	**-2.40**	**3.57**	**-8.06**	**0.88**	**-0.005**	**1.5**	**0.99**	**40**
36.7	**36.8**	**1279**	**147**	**0.88**	**-**	**20.18**	**-**	**1.05**	**0.003**	**1.0**	**1.0**	**44**

			1		3.58		7.86				0	
36.8	36.9	1531	4683	1.43	-2.57	-74.16	17.14	0.45	0.003	1.2	1.00	58
36.9	36.9	1614	4840	1.12	-2.24	-77.82	10.87	0.45	0.001	1.2	1.00	31
36.9	37.0	1946	7686	1.50	-4.85	-158.89	19.19	0.45	0.003	2.3	1.00	109
37.0	37.1	2586	6937	0.90	-3.65	-137.01	8.11	0.63	0.002	0.7	1.00	71
						Sigma-4						
37.1	45.9	3050	1808	0.35	0.79	10.42	-15.68	0.42	-0.005	0.7	0.99	174
45.9	46.0	3730	3087	0.29	-0.49	-27.18	-8.62	0.75	0.001	1.2	1.00	122
46.0	46.0	4195	-14016	0.43	3.45	460.19	-21.03	1.04	0.005	1.4	1.00	43

46.0	**46.1**	**4582**	**-6879**	**0.40**	**-0.61**	**258.02**	**23.20**	**1.15**	**0.005**	**1.0**	**0.99**	**68**
46.1	**60.0**	**5108**	**42132**	**-0.63**	**-0.99**	**-1154.59**	**28.25**	**1.85**	**0.011**	**1.1**	**0.89**	**62**

Table 1b.

Min density	Max density	Mean Layer Depth (m)	a	$Si(OH)_4$	NO_3	Sal	Theta	AOU	Pressure	rmse	R^2	n
Sigma-θ												
20.0	23.5	31	263	7.28	-96.35	43.77	5.95	-0.20	-0.047	8.6	0.92	42
23.5	24.5	50	466	-8.70	29.32	44.65	-1.93	0.50	0.024	8.4	0.93	150
24.5	25.0	53	1052	-0.11	5.00	28.96	-2.49	0.45	0.107	2.9	0.99	56
25.0	25.4	57	1259	-3.68	2.04	22.21	-0.65	0.62	0.212	6.4	0.95	57
25.4	26.2	107	974	1.55	2.21	31.43	-2.76	0.53	0.061	6.8	0.98	137
26.2	26.4	160	1097	0.62	2.93	27.82	-1.96	0.43	0.008	3.8	0.99	75
26.4	26.6	196	964	0.58	3.55	31.3	-	0.29	0.015	3.4	0.9	89

						6	1.47				9	
26.6	26.8	259	1326	0.88	4.27	19.87	1.84	0.17	0.005	2.5	1.00	104
26.8	27.0	310	1405	1.00	3.92	17.82	1.83	0.18	-0.001	2.5	1.00	150
27.0	27.2	431	1448	0.84	3.36	17.21	0.64	0.22	-0.004	3.5	0.99	197
27.2	27.4	672	1331	0.66	2.29	21.80	-2.33	0.32	-0.004	3.4	0.99	272
27.4	27.5	991	1109	0.76	1.39	28.96	-3.64	0.37	-0.004	4.2	0.75	74
Sigma-2												
27.5	36.7	1108	1915	0.41	1.44	5.68	-3.05	0.37	0.005	2.0	0.98	90
36.7	36.8	1279	1272	0.53	0.47	25.06	-8.77	0.55	-0.002	1.7	1.00	32
36.8	36.9	1531	1473	0.76	1.57	18.17	-0.31	0.30	-0.003	5.3	0.98	105
36.9	36.9	1614	3278	0.82	1.18	-33.66	4.65	0.20	-0.002	2.8	0.99	94
36.9	37.0	1946	4372	0.76	1.43	-65.0	5.14	0.11	0.001	2.2	1.00	226

						8						
37.0	**37.1**	**2586**	**3899**	**0.36**	**1.15**	**-51.16**	**-1.59**	**0.43**	**0.002**	**1.9**	**1.00**	**194**
						Sigma-4						
37.1	**45.9**	**3050**	**1335**	**0.53**	**2.11**	**21.83**	**-2.35**	**0.29**	**0.002**	**1.7**	**0.98**	**145**
45.9	**46.0**	**3730**	**3036**	**0.64**	**1.53**	**-27.11**	**4.95**	**0.21**	**0.003**	**1.8**	**1.00**	**268**
46.0	**46.0**	**4195**	**8008**	**0.09**	**1.73**	**-168.68**	**-0.95**	**0.23**	**0.003**	**2.6**	**0.99**	**75**
46.0	**46.1**	**4582**	**810**	**0.06**	**0.32**	**38.12**	**-13.29**	**0.77**	**0.005**	**3.0**	**0.60**	**165**
46.1	**60.0**	**5108**	**-5867**	**0.00**	**0.30**	**230.89**	**-27.07**	**0.80**	**0.003**	**1.2**	**0.74**	**108**

Table 2.

Water Mass	Density Range	Latitude	Pressure (dbar)	dC_{ant}/dt (µmol kg^{-1} yr^{-1})	dC_{ant}/dt^{a} (µmol kg^{-1} yr^{-1})	dpH/dt (yr^{-1})
SACW	$\sigma^{\theta}20$ - $\sigma^{\theta}26.8$	23° S - 18° S	90-160	0.99±0.14	0.90±0.04	-0.0016
SAMW	$\sigma^{\theta}26.8$ - $\sigma^{\theta}27.1$	50° S – 48° S	90-160	0.53±0.11	0.53±0.02	-0.0014
AAIW	$\sigma^{\theta}27.1$ - $\sigma^{\theta}27.4$	50° S – 48° S	360-450	0.36±0.06	0.36±0.06	-0.0010
*u*CDW	$\sigma^{\theta}27.4$ - $\sigma^{3}41.47$	50° S – 49° S	1400-1800	0.33±0.07	0.16±0.04	-0.0010
*u*NADW	$\sigma^{\theta}27.4$ - $\sigma^{3}41.47$	10° N – 15° N	1600-1800	0.20±0.03	0.16±0.04	-0.0005
*l*CDW	$\sigma^{3}41.47$ - $\sigma^{4}45.9$	50° S – 48° S	3250-3750	0±0.06	0.08±0.04	0.0000
*l*NADW	$\sigma^{3}41.47$ - $\sigma^{4}45.9$	10° N – 15° N	3000-3500	0±0.02	0.08±0.04	0.0000

Table 3.

Water Mass	**Salinity**	**Theta (°C)**	**γDIC (mmol kg^{-1})**	**βDIC (mmol kg^{-1})**	**ωDIC (mmol kg^{-1})**	**Revelle Factor**
SACW	**36.854**	**22.693**	**0.211**	**0.256**	**-0.327**	**10.02**
SAMW	**34.021**	**4.4218**	**0.144**	**0.161**	**-0.181**	**14.83**
AAIW	**34.222**	**2.8567**	**0.136**	**0.149**	**-0.165**	**16.02**
***u*CDW**	**34.682**	**1.9528**	**0.132**	**0.143**	**-0.156**	**17.14**
***u*NADW**	**34.987**	**3.8578**	**0.132**	**0.168**	**-0.191**	**14.40**

Table Captions

Table 1. Calculated coefficients for the performed multi linear regressions for each density interval using the (a) GEOTRACES-NL (2010/2011) dataset and (b) WOCE ’94 A17 dataset. Differences between the coefficients were calculated following equation (2).

Table 2. The calculated rates of increase of C_{ant} and rates of decrease of pH along the section, listed per water mass. The identification criteria for each water mass are provided. Error represents $2\sigma/N^{0.5}$. [a]Values from Ríos et al. [2012].

Table 3. The average water mass values of salinity and potential temperature, with accompanying average buffering capacity values (γDIC, βDIC, ωDIC and revelle factor) calculated using the GEOTRACES-NL (2010/11) dataset. Water masses are determined using the same criteria as given in Table 2.

Figure Captions

Figure 1. Stations where DIC and A_T samples were taken from both cruises (black represents the WOCE '94 A17 stations, red represents the GEOTRACES-NL (2010/2011) expeditions).

Figure 2. The residuals of the MLR fits of the (a) WOCE '94 A17 and (b) GEOTRACES-NL (2010/2011) datasets.

Figure 3. Section distributions of temperature (ºC), salinity, AOU (μmol kg^{-1}), silicate (μmol kg^{-1}), A_T (μmol kg^{-1}) and DIC (μmol kg^{-1}) from the GEOTRACES-NL (2010/2011) dataset.

Figure 4. (a) Distribution of C_{ant} (μmol kg^{-1}) calculated using the φC_T^0 method with the GEOTRACES-NL (2010/2011) dataset, (b) Distribution of $\Delta C_{ant}^{1994\text{-}2011}$ (μmol kg^{-1}), calculated using the eMLR approach, (c) Distribution of the $\Delta pH^{1994\text{-}2011}$ associated with

$\Delta C_{ant}^{1994\text{-}2011}$. The aragonite saturation horizon (ΩAr) is marked on for pre-industrial times (solid line), 1994 (dashed line) and 2011 (dotted line).

Figure 5. Distribution of the (a) Revelle factor across the section and the three buffering factors relating to DIC; (b) βDIC, (c) γDIC, and (d) ωDIC. The latter three are all given in mmol kg^{-1}.

Figure 6. The buffer factors βDIC (top), γDIC (middle), and ωDIC(bottom) of each water mass over a range of DIC concentrations. The vertical lines denote the DIC concentration in pre-industrial times, 1994, 2011 and the projected concentration in 2110.

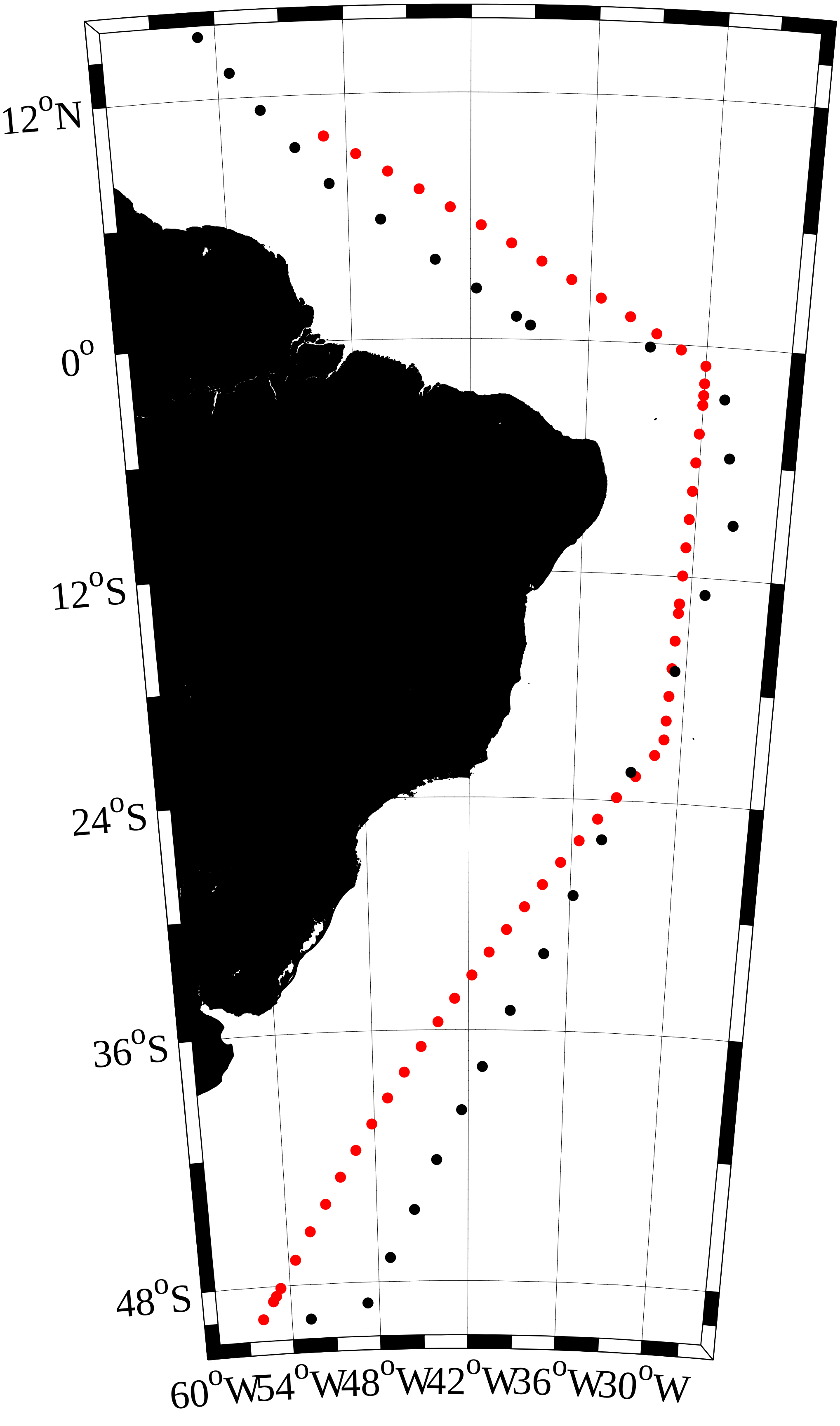
12°N
0°
12°S
24°S
36°S
48°S
60°W
54°W
48°W
42°W
36°W
30°W

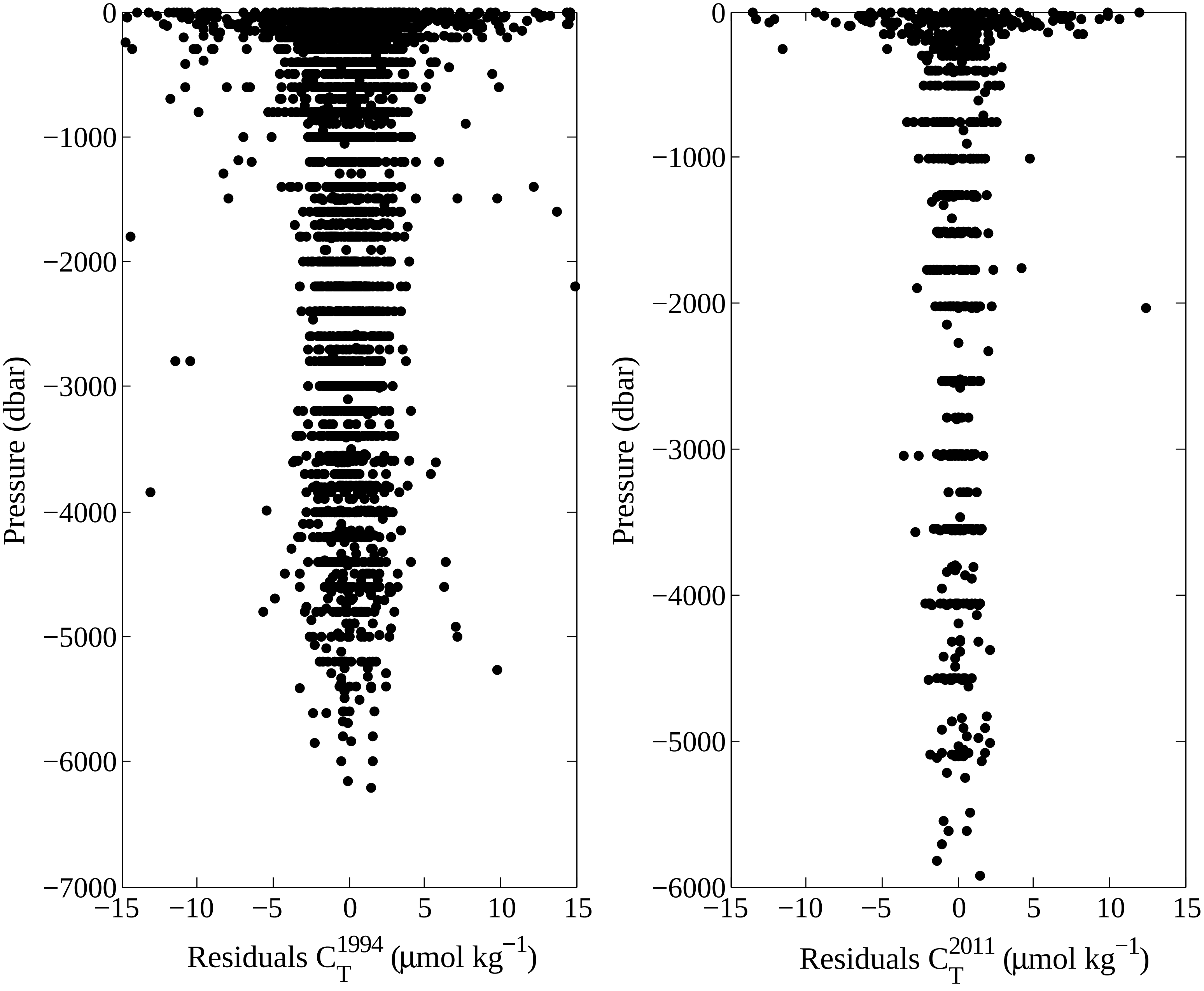
Pressure (dbar)
0
−1000
−2000
−3000
−4000
−5000
−6000
−7000
−15
−10
−5
0
5
10
15
Residuals C_T^{1994} (μmol kg^{-1})
Pressure (dbar)
0
−1000
−2000
−3000
−4000
−5000
−6000
−15
−10
−5
0
5
10
15
Residuals C_T^{2011} (μmol kg^{-1})

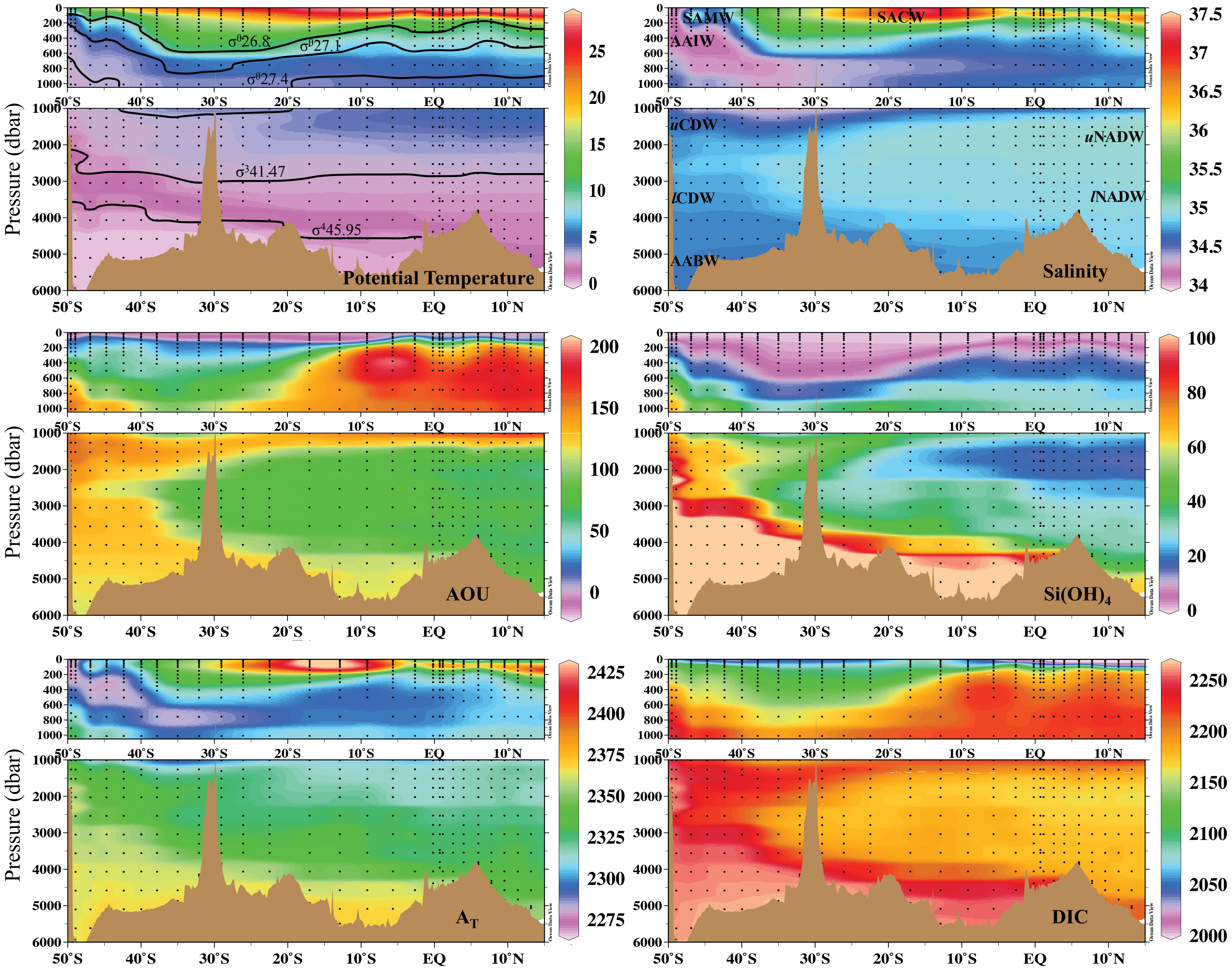
Potential Temperature
Salinity
AOU
Si(OH)4
A_T
DIC
Pressure (dbar)
σθ26.8
σθ27.1
σθ27.4
σ341.47
σ445.95
SAMW
SACW
AAIW
uCDW
uNADW
lCDW
lNADW
AABW
50°S
40°S
30°S
20°S
10°S
EQ
10°N
0
200
400
600
800
1000
2000
3000
4000
5000
6000
25
20
15
10
5
0
37.5
37
36.5
36
35.5
35
34.5
34
200
150
100
50
0
100
80
60
40
20
0
2425
2400
2375
2350
2325
2300
2275
2250
2200
2150
2100
2050
2000
Ocean Data View

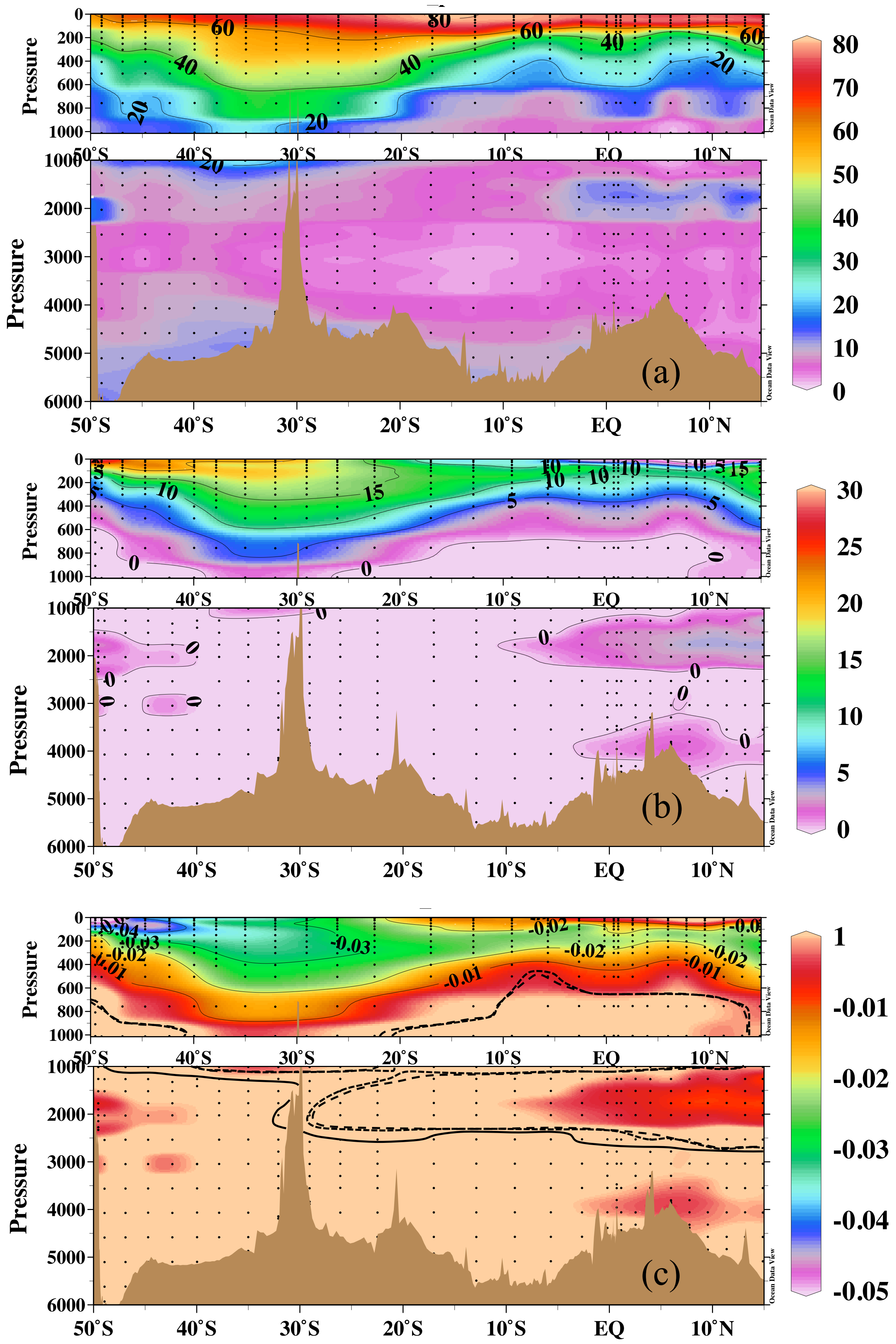
Pressure
0
200
400
600
800
1000
2000
3000
4000
5000
6000
50°S
40°S
30°S
20°S
10°S
EQ
10°N
80
70
60
50
40
30
20
10
0
(a)
30
25
15
5
(b)
1
-0.01
-0.02
-0.03
-0.04
-0.05
(c)
Ocean Data View

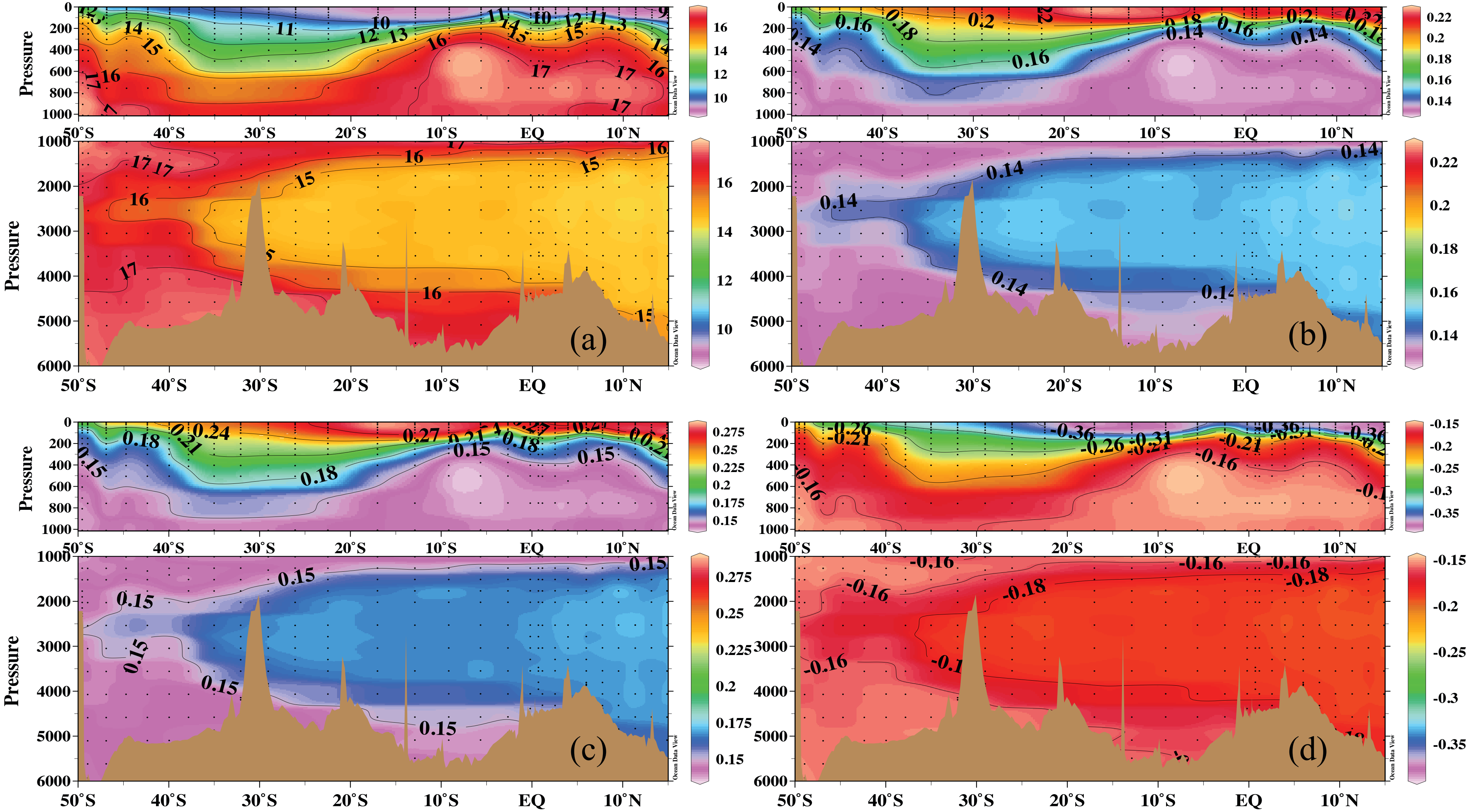
(a)
(b)
(c)
(d)
Pressure
0
200
400
600
800
1000
2000
3000
4000
5000
6000
50°S
40°S
30°S
20°S
10°S
EQ
10°N
16
14
12
10
0.22
0.2
0.18
0.16
0.14
0.275
0.25
0.225
0.2
0.175
0.15
-0.15
-0.2
-0.25
-0.3
-0.35
Ocean Data View

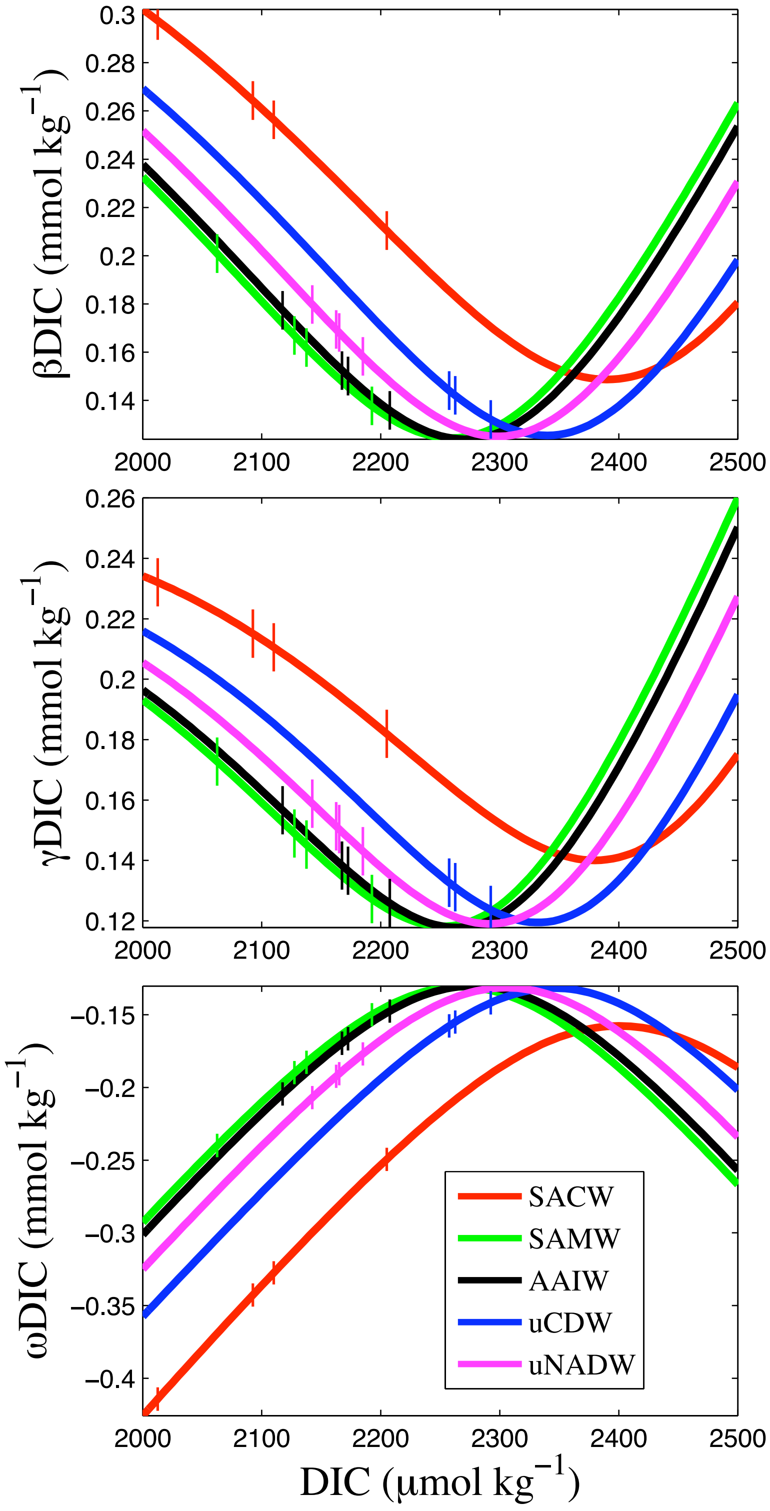
βDIC (mmol kg^{-1})
0.3
0.28
0.26
0.24
0.22
0.2
0.18
0.16
0.14
2000
2100
2200
2300
2400
2500
γDIC (mmol kg^{-1})
0.26
0.24
0.22
0.2
0.18
0.16
0.14
0.12
2000
2100
2200
2300
2400
2500
ωDIC (mmol kg^{-1})
−0.15
−0.2
−0.25
−0.3
−0.35
−0.4
2000
2100
2200
2300
2400
2500
DIC (μmol kg^{-1})
SACW
SAMW
AAIW
uCDW
uNADW